Atmospheric Environment 182 (2018) 31–40

Contents lists available at ScienceDirect

Atmospheric Environment

journal homepage: www.elsevier.com/locate/atmosenv

# Daytime variation of aerosol optical depth in North China and its impact on aerosol direct radiative effects

Jingjing Song[a,b], Xiangao Xia[a,b,c,*], Huizheng Che[d,**], Jun Wang[e], Xiaoling Zhang[f], Xiaojing Li[g]

[a] LAGEO, Institute of Atmospheric Physics, Chinese Academy of Sciences, Beijing, 100029, China
[b] College of Earth Sciences, University of Chinese Academy of Sciences, Beijing, 100049, China
[c] Collaborative Innovation Center on Forecast and Evaluation of Meteorological Disasters, Nanjing University of Information Science & Technology, Nanjing, 210044, China
[d] State Key Laboratory of Severe Weather (LASW) and Institute of Atmospheric Composition, Chinese Academy of Meteorological Sciences (CAMS), CMA, Beijing, 10081, China
[e] Department of Chemical and Biochemical Engineering, Center for Global and Regional Environmental Studies, and Informatics Initiative, University of Iowa, Iowa City, IA 52241, USA
[f] School of Atmospheric Sciences, Plateau Atmosphere and Environment Key Laboratory of Sichuan Province, Chengdu University of Information Technology, Chengdu, 610225, China
[g] National Satellite Meteorological Center, China Meteorological Administration, Beijing, 100082, China

## GRAPHICAL ABSTRACT

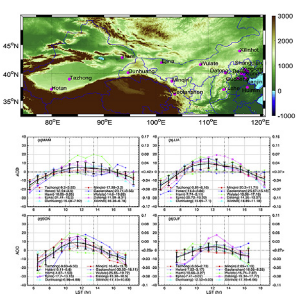

## ARTICLE INFO

*Keywords:*
Daytime variation
Aerosol optical depth
Direct radiative effects
North China

## ABSTRACT

Daytime cycles of aerosol optical depth (AOD) and Angstrom exponent (AE) climatology were analyzed based on long-term (5–15 years) measurements at 18 stations of the China Aerosol Remote Sensing Network (CARSNET) in North China. AOD in Northwest China (NWC) exhibits a daytime trend with negative departures in the early morning and later afternoon while positive departures at midday. Daytime AOD relative departure in different sites and seasons varies from −30.26% to 30.28%. AE in NWC shows an opposite pattern to daytime variation of AOD. Daytime variation of AE is negligible in North China Plain (NCP), AOD increases steadily throughout the day. This trend is consistent and repeatable in four seasons. Such pronounced variability in AOD and AE should be taken accounted for in the estimation of diurnal aerosol direct radiative effects (ADRE), as suggested by the radiative transfer model simulations. The replacement of the observed daytime variation of AOD and AE by daytime mean values in NWC results in ADRE differences of 0.31 $Wm^{-2}$ at the surface and 0.05 $Wm^{-2}$ at the top of the atmosphere (TOA). ADRE in NWC will be underestimated by −0.47 $Wm^{-2}$ and -0.25 $Wm^{-2}$ at the surface and TOA, respectively, if instantaneous AOD and AE during the overpass time of Terra and Aqua are taken as the daytime mean values. The annual mean ADRE at the surface and TOA will be underestimated by −0.17 $Wm^{-2}$ and -0.03 $Wm^{-2}$ if daytime variations of AOD and AE are replaced by daytime mean values in NCP. ADRE will be

* Corresponding author. LAGEO, Institute of Atmospheric Physics, Chinese Academy of Sciences, China.
** Corresponding author.
*E-mail addresses:* xxa@mail.iap.ac.cn (X. Xia), chehz@cma.gov.cn (H. Che).

https://doi.org/10.1016/j.atmosenv.2018.03.024
Received 2 October 2017; Received in revised form 27 February 2018; Accepted 11 March 2018
Available online 12 March 2018

underestimated by $-0.07\ Wm^{-2}$ at the surface and $-0.06\ Wm^{-2}$ at the TOA if instantaneous AOD and AE during the overpass time of Terra and Aqua other than daytime variation of AOD and AE are used in the calculations.

## 1. Introduction

Tropospheric aerosols are highly variable in time and space, which is closely related to emissions from diverse origins, meteorological processes on various scales, chemical evolution and removal processes. Comprehensive understanding of aerosol properties and their spatial and temporal variations on various scales is fundamental for further understanding of aerosol's effects on climate and environment. Ground based remote sensing is an essential method to characterize aerosol optical properties and has been playing an important role in aerosol research (Holben et al., 2001). Aerosol optical properties retrieved from ground Sun-photometer measurements are characterized by higher temporal resolution (minutes) as compared with satellite remote sensing (hours to days), which is valuable for revealing subtle variation of aerosol optical properties at a local scale (Che et al., 2011, 2014; Zhu et al., 2014).

Much progress has been made in ground remote sensing of aerosol optical properties in China during the last decade. Chinese Meteorological Administration initiated a ground network (the China Aerosol Remote Sensing Network, CARSNET) to remote sensing dust aerosols in 2002 when abnormally frequent dust outbreaks occurred. The CARSNET was originally composed of 20 stations in Northwest China and expanded to include more than 50 stations across the country in the present (Che et al., 2009, 2015a). Spatial distribution and seasonal variation of aerosol optical depth (AOD) was studied based on ten years CARSNET data (Che et al., 2014, 2015b; Xia et al., 2016). Significant effects of dust events in spring, hygroscopic growth in summer and biomass burning during the crop harvest season on aerosol loading were recorded by the CARSNET data.

Various applications need information on daytime variability of AOD, for instance, the representativeness of snapshot of aerosol properties in depicting daytime mean aerosol loading and direct radiative effects from polar satellites (Kaufman et al., 2000; Wang et al., 2015). Major factors contributing to aerosol daytime variations include emission (Wang et al., 2006), meteorology (transport and deposition, Wang et al., 2003), photochemistry and hygroscopic growth (Wang and Martin, 2007). More importantly, several factors usually work together to determine the aerosol daytime variation (Zhang et al., 2012). Substantially different daytime variations of AOD for different aerosol types and surface landscapes were found based on multi-site multi-year AOD data from the aerosol robotic network (AERONET) (Smirnov et al., 2002), which indicated a large spatial and seasonal dependence of daytime variation.

In China, daytime variation of AOD was for the first time studied by using 22 months of Sun-photometer AOD measurements at Dunhuang, Northwest China (Wang et al., 2004), which showed a distinct daytime variation of AOD and Angstrom exponent (AE). More specific, season-invariant daytime change of more than 40% for AOD and 30% for AE. Larger AOD but smaller AE values were generally observed late in the afternoon (Che et al., 2013). Daytime AOD at Beijing increases persistently and the daytime variation varies from 15% in summer to 45% in winter (Xia et al., 2006).

Diurnal mean aerosol direct radiative effects (ADRE, defined here as the differences in clear sky solar radiation at the top and bottom of the atmosphere in the presence and absence of aerosols), as a result of aerosol direct scattering and absorbing of solar radiation, are highly dependent on aerosol optical properties and their temporal variations (Christopher et al., 2003). ADRE calculated from diurnal mean aerosol optical properties would likely be substantially different from that based on instantaneous aerosol optical properties if they show remarkable diurnal variations (Wang et al., 2004). More specific, one would expect much stronger impact at individual sites where either maximum or minimum AOD occurs at nearly local noon. For example, ADRE at the top of the atmosphere bias varied from $-7.6$–$15.6\ W\,m^{-2}$ for heavy aerosol loading, if diurnal mean values of AOD and aerosol intensive properties including single scattering albedo (SSA) and asymmetry factor (ASY) other than time-resolved observations were used in the calculations of ADRE (Wang et al., 2015). The diurnal variation of AOD in North China tended to cause a bias of ADRE on both seasonal and annual scales up to $2.2 \pm 3.9\ W\,m^{-2}$ at the top of the atmosphere (TOA) and abnormally high value of $43.7 \pm 72.7\ W\,m^{-2}$ at the surface if satellite snapshot AOD was used to represent the diurnal average (Xu et al., 2016). Surface aerosol extinction, SSA and ASY at a rural station in North China show a substantial diurnal variation likely as a result of hygroscopic growth of ambient aerosols. While ADRE estimation would be improved if both aerosol optical properties averaged over early morning and late afternoon were used, otherwise, a bias of ADRE would be expected (Kuang et al., 2015). This indicated that diurnal AOD variability did not typically result in a significant impact on diurnal mean ADRE estimates if the morning and afternoon AOD patterns were opposite and thus the impact on ADRE, when integrated over all solar zenith angles, was reduced (Arola et al., 2013).

North China (75°～120° E; 35°～42° N) is outstanding since this region is characterized by distinct anthropogenic and natural aerosol sources that show seasonal and regional dependence. Variation of AOD and AE may show substantial regional and seasonal dependence, which is not clear up to the present and thereby needs further study. The CARSNET measurements with a good spatial and temporal coverage during the last decade provide an opportunity to study how aerosol optical properties vary in this key region, which will certainly shed new light on the regional and seasonal dependence of ADRE on daytime variation of aerosol optical properties.

The objective of this study is to present the climatology of daytime variation of AOD and AE in North China. The spatial and seasonal dependences of daytime variation will be studied in detail. Furthermore, effects of daytime variations of AOD and AE on ADRE are presented. While these two topics have been preliminarily studied, this paper differs in following ways from previous studies. Firstly, the research is, for the first time, based on aerosol data at 18 stations in North China that favors for a clear picture of daytime variation at a regional scale. Secondly, effect of daytime variation AOD on surface solar radiation is discussed since solar energy is one of important renewable energies and application of solar energy has advanced rapidly in China. North China is characterized by rich solar energy resource, potential uncertainty of assessment of solar energy source associated with aerosol data from polar satellite is evaluated. Thirdly, potential impacts of uneven data sampling of aerosol on the calculation of daytime variation and therefore aerosol direct radiative forcing are addressed.

## 2. Site, data and method

### 2.1. Site and data

CIMEL Sun-photometer (Cimel Electronique, CE-318), the standard instrumentation for the AERONET, was installed at 18 stations as a part of CARSNET or AERONET in North China. Since the original objective the CARSNET is to detect dust, most stations in Northwest China (NWC) are located in dust source or downwind regions (shown in Fig. 1). For example, Tazhong station is located in the Taklimakan Desert, the

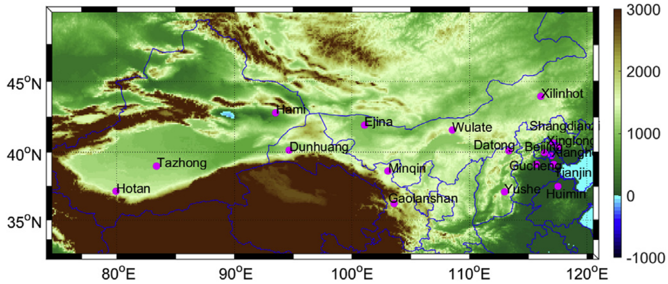


**Fig. 1.** Spatial distribution of 18 CARSNET and AERONET stations (dots) overlapped on the terrain (color map). (For interpretation of the references to color in this figure legend, the reader is referred to the Web version of this article.)

major dust source region of East Asia. In North China Plain (NCP), stations are installed at diverse landscapes, for example, in mega-cities (Beijing and Tianjing), rural region (Xianghe and Gucheng) and background region (Shangdianzi and Xinglong, at the top of mountains). Stations are grouped into two categories according to their location and dominant aerosol types: stations in NWC characterized by dust aerosols and stations in NCP characterized by a mixture of anthropogenic and natural aerosols (Table 1). This classification is also supported by the fact that daytime variations of AOD and AE are similar among individual sites within each region.

CIMEL Sun-photometer make direct spectral solar radiation measurements in a 1.2° full field of view every nominal 15 min (Holben et al., 1998; Che et al., 2009). A few CIMEL types that differ in wavelength and data collection techniques are used in the CARSNET and AERONET. AODs at 4 wavelengths (the standard wavelengths for all CIMEL types), i.e., 440, 675, 870 and 1020 nm available for all stations are used to interpolate AOD at 550 nm and calculate AE. The master CIMEL of the CARSNET is calibrated using the Langley method at either Izana, Spain (28.31° N, 16.50° W, 2931 m.s.l.) or Mauna Loa, USA (19.54° N, 55.58° W, 3397 m.s.l.). The field instruments are calibrated by inter-comparison with the master in Beijing at least once a year following the AERONET calibration protocol (Che et al., 2009). Inter-comparison of AODs from CARSNET and AERONET in Beijing showed that the former were larger than the latter by 0.03, 0.01, 0.01 and 0.01 at wavelengths of 1020, 870, 670 and 440 nm (Che et al., 2009). The uncertainty of AE depends on AOD, i.e., the larger AOD, the smaller uncertainty of AE and vice versa.

### 2.2. *Daytime variations of AOD and AE and their impacts on ADRE*

Previous seasonal daytime variations of AOD and AE were generally calculated as follows (Smirnov et al., 2002; Wang et al., 2004; Peterson et al., 1981). Instantaneous departures for a day are calculated firstly as a percentage departure from the daily mean (calculated from all individual observations), which are then used to calculate hourly departures for a day. Seasonal mean variations are finally calculated from hourly departures of all days in each season. This method will often lead to a result that the sum of hourly departures for a day does not equal zero due to uneven distribution of AOD and AE (the amount of valid AOD and AE in each hour is different because of cloud contamination). Therefore, we adopt a slightly different method to modify the calculation of daily daytime variations through shifting hourly AOD values by their mean value. Solar radiation at the surface and TOA is calculated based on the Santa Barbara DISORT (discrete ordinates radiative transfer) Atmospheric Radiative Transfer (SBDART) model (Ricchiazzi et al., 1998). Inputs of aerosol properties into the model include AOD, SSA, ASY, surface albedo at 4 wavelengths (440, 670, 870, 1020 nm) of the CIEML Sun-photometer and AE. Since SSA and ASY are not yet available at the CARSNET stations, the climatological values of SSA and ASY retrievals at SACOL and Beijing are used to represent optical properties at stations in NWC and NCP, respectively. It is

**Table 1**
Diurnally averaged AOD, AE and detail information including location and study period for each site.

| Site | Latitude, longitude | Study period | Effective days | Averaged AOD | | | | Averaged AE | | | |
|---|---|---|---|---|---|---|---|---|---|---|---|
| | | | | Spring | Summer | Autumn | Winter | Spring | Summer | Autumn | Winter |
| **NWC** | | | | | | | | | | | |
| Tazhong | 39.0°N, 83.4°E | 2004.01–2012.04 | 2140 | 0.73 ± 0.08 | 0.64 ± 0.04 | 0.34 ± 0.04 | 0.29 ± 0.01 | 0.11 ± 0.01 | 0.14 ± 0.01 | 0.34 ± 0.07 | 0.49 ± 0.05 |
| Hotan | 37.1°N,79.9°E | 2002.05–2005.03 | 756 | 0.64 ± 0.08 | 0.68 ± 0.07 | 0.41 ± 0.02 | 0.29 ± 0.03 | 0.10 ± 0.03 | 0.10 ± 0.04 | 0.21 ± 0.05 | 0.50 ± 0.05 |
| Hami | 42.8°N,93.5°E | 2002.04–2005.03 | 835 | 0.27 ± 0.02 | 0.18 ± 0.01 | 0.16 ± 0.01 | 0.24 ± 0.02 | 0.59 ± 0.09 | 0.71 ± 0.07 | 0.60 ± 0.06 | 0.61 ± 0.03 |
| Ejina | 41.9°N,101.1°E | 2002.05–2012.04 | 2561 | 0.30 ± 0.02 | 0.23 ± 0.03 | 0.15 ± 0.01 | 0.15 ± 0.01 | 0.38 ± 0.03 | 0.55 ± 0.06 | 0.73 ± 0.04 | 0.66 ± 0.04 |
| Dunhuang | 40.2°N,94.7°E | 2002.06–2011.12 | 2687 | 0.42 ± 0.06 | 0.28 ± 0.02 | 0.19 ± 0.01 | 0.24 ± 0.01 | 0.31 ± 0.06 | 0.36 ± 0.08 | 0.53 ± 0.06 | 0.62 ± 0.07 |
| Minqin | 38.6°N,103.1°E | 2004.02–2012.04 | 1683 | 0.40 ± 0.03 | 0.39 ± 0.04 | 0.29 ± 0.03 | 0.26 ± 0.02 | 0.35 ± 0.04 | 0.47 ± 0.08 | 0.55 ± 0.10 | 0.64 ± 0.07 |
| Gaolanshan | 36.2°N,103.6°E | 2004.06–2012.04 | 1137 | 0.46 ± 0.05 | 0.33 ± 0.04 | 0.34 ± 0.06 | 0.37 ± 0.04 | 0.59 ± 0.07 | 0.87 ± 0.06 | 0.85 ± 0.10 | 0.83 ± 0.08 |
| Wulate | 41.6°N,108.5°E | 2002.04–2005.02 | 894 | 0.30 ± 0.04 | 0.29 ± 0.03 | 0.19 ± 0.02 | 0.19 ± 0.01 | 0.64 ± 0.14 | 0.86 ± 0.07 | 0.70 ± 0.08 | 0.74 ± 0.09 |
| Datong | 40.1°N,113.3°E | 2002.05–2012.04 | 2571 | 0.41 ± 0.02 | 0.43 ± 0.05 | 0.36 ± 0.04 | 0.42 ± 0.06 | 0.72 ± 0.05 | 0.94 ± 0.07 | 0.89 ± 0.04 | 0.85 ± 0.02 |
| Xilinhot | 43.9°N,116.1°E | 2002.04–2012.04 | 2493 | 0.28 ± 0.01 | 0.26 ± 0.03 | 0.16 ± 0.01 | 0.16 ± 0.01 | 0.70 ± 0.09 | 0.78 ± 0.13 | 0.77 ± 0.13 | 0.67 ± 0.09 |
| **NCP** | | | | | | | | | | | |
| Beijing | 40.0°N,116.4°E | 2001.03–2014.01 | 3035 | 0.55 ± 0.06 | 0.59 ± 0.07 | 0.40 ± 0.04 | 0.33 ± 0.04 | 0.98 ± 0.02 | 1.27 ± 0.05 | 1.17 ± 0.03 | 1.10 ± 0.01 |
| Xianghe | 39.8°N,117.0°E | 2001.03–2012.05 | 1973 | 0.50 ± 0.06 | 0.66 ± 0.15 | 0.39 ± 0.03 | 0.28 ± 0.02 | 1.02 ± 0.05 | 1.26 ± 0.05 | 1.19 ± 0.04 | 1.09 ± 0.02 |
| Xinglong | 40.4°N,117.6°E | 2006.02–2012.05 | 1160 | 0.33 ± 0.06 | 0.33 ± 0.07 | 0.17 ± 0.02 | 0.16 ± 0.04 | 0.98 ± 0.03 | 1.27 ± 0.06 | 1.23 ± 0.04 | 1.09 ± 0.04 |
| Yushe | 37.1°N,113.0°E | 2005.06–2012.04 | 1539 | 0.45 ± 0.03 | 0.53 ± 0.07 | 0.36 ± 0.05 | 0.33 ± 0.03 | 0.79 ± 0.03 | 1.19 ± 0.07 | 1.12 ± 0.10 | 1.03 ± 0.08 |
| Shangdianzi | 40.7°N,117.1°E | 2004.03–2012.04 | 2107 | 0.41 ± 0.04 | 0.44 ± 0.03 | 0.30 ± 0.02 | 0.24 ± 0.01 | 0.99 ± 0.04 | 1.20 ± 0.02 | 1.19 ± 0.03 | 1.10 ± 0.05 |
| Gucheng | 39.1°N,115.7°E | 2007.10–2012.03 | 1007 | 0.54 ± 0.05 | 0.52 ± 0.03 | 0.40 ± 0.06 | 0.50 ± 0.04 | 1.10 ± 0.07 | 1.29 ± 0.09 | 1.34 ± 0.06 | 1.25 ± 0.10 |
| Tianjin | 39.1°N,117.2°E | 2002.04–2012.04 | 1868 | 0.57 ± 0.03 | 0.62 ± 0.04 | 0.48 ± 0.06 | 0.42 ± 0.03 | 0.92 ± 0.03 | 1.07 ± 0.07 | 1.13 ± 0.05 | 1.05 ± 0.05 |
| Huimin | 37.5°N,117.5°E | 2007.04–2012.04 | 923 | 0.50 ± 0.03 | 0.54 ± 0.02 | 0.46 ± 0.02 | 0.44 ± 0.03 | 0.97 ± 0.04 | 1.20 ± 0.05 | 1.27 ± 0.03 | 1.11 ± 0.04 |

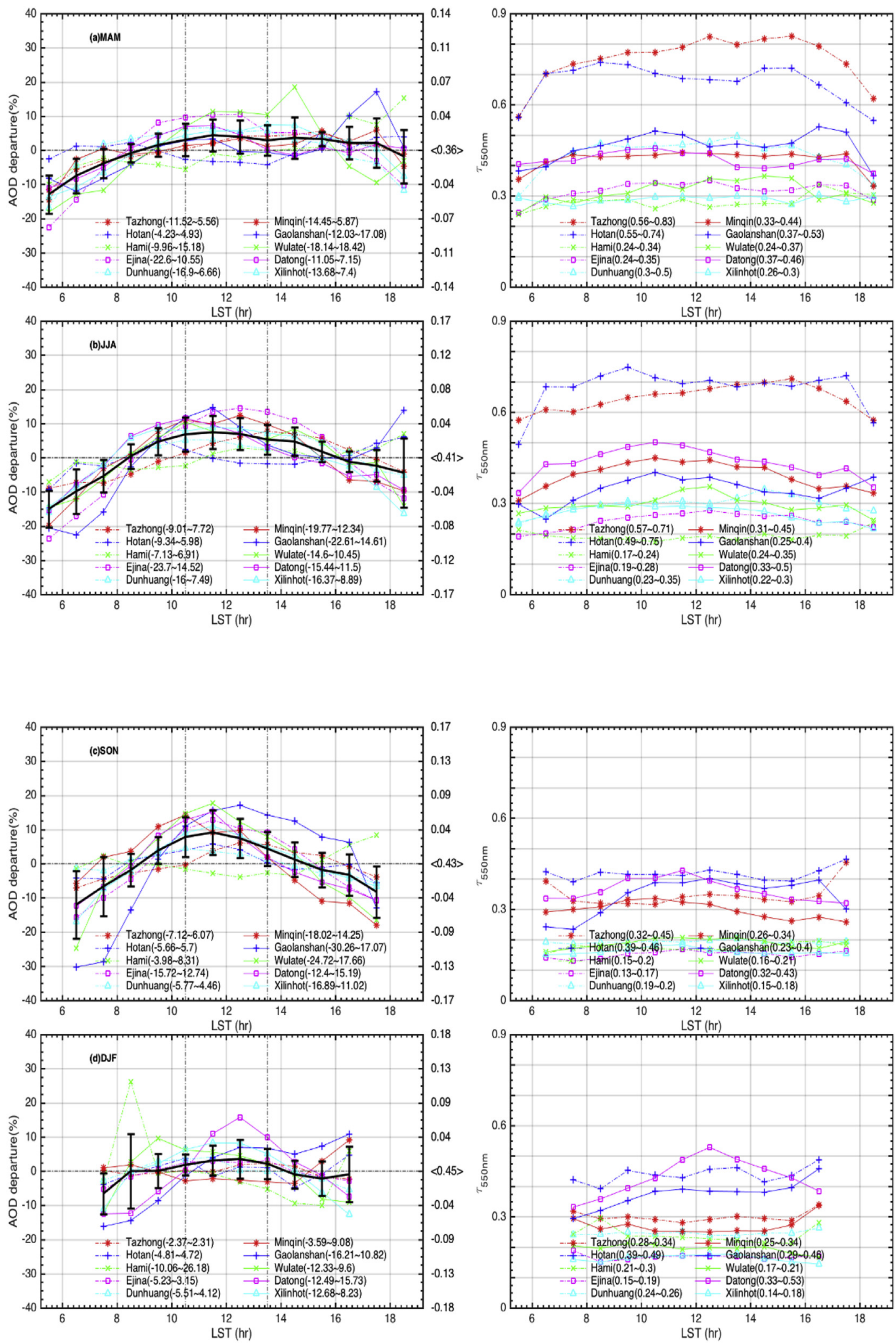

**Fig. 2.** Daytime variability of aerosol optical depth in spring (a), summer (b), autumn (c) and winter (d) at 10 stations in Northwest China. In the first column, the left axis indicates the relative departure of AOD and average AOD in NWC region is given on right hand axis (absolute deviation AOD values from the daytime average in NWC also showed on the right y axis). The specific variation range of relative departure of AOD in each site are list next to the site names. The second column represents the absolute hourly observed AOD in each site corresponding to four seasons. The dotted lines in left (right) indicate Terra (Aqua) overpass time.

assumed that the surface albedo in each site is constant throughout a day. In addition, the atmospheric profile of standard middle-latitude atmosphere is used in the calculations. The SBDART is run with a 1-h time step over a 24 h diurnal cycle on 15th January, April, July and October to represent the seasonal averages in winter, spring, summer and fall, respectively. Five simulations are performed with input of different daytime variations of AOD and AE to the SBDART to calculate potential ADRE differences as a result of different scenarios of daytime aerosol variations.

S1: observed hourly AOD and AE as a reference;

S2: CARSNET observed daytime mean AOD and AE;

S3: CARSNET observed instantaneous AOD and AE at the Terra and overpass time (~10:30 and ~13:30 local time);

S4: observed daytime variation of AOD but daytime mean AE;

S5: observed daytime variation of AE but daytime mean AOD;

Potential differences in the calculations of solar radiation at the surface or at TOA from S2 to S5 to that from the S1 reflect how much ADRE is impacted if actual aerosol daytime variations are not

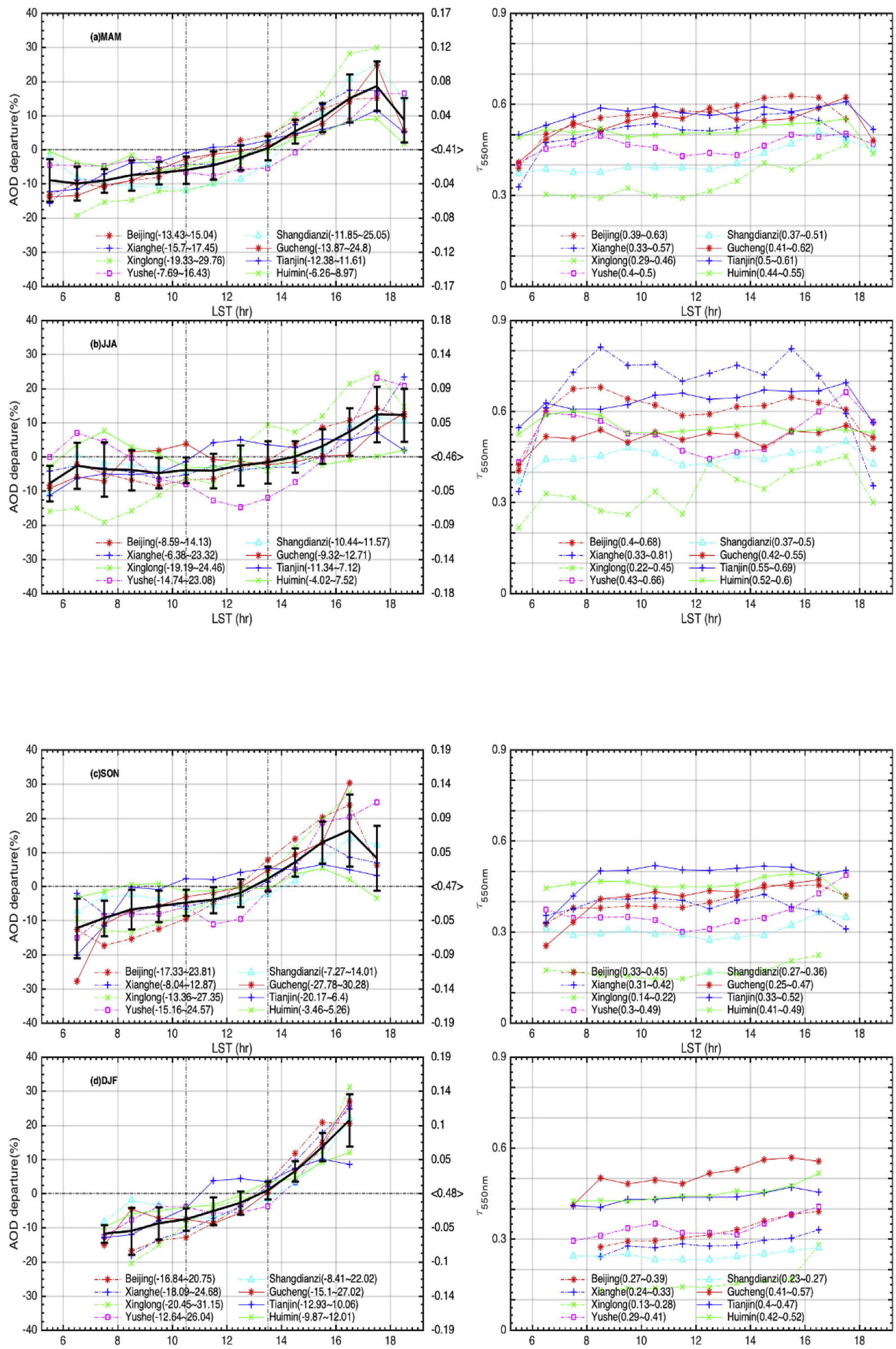


**Fig. 3.** Similar to Fig. 2 but for 8 stations in North China Plain.

considered. Note that the objective of S4 and S5 is to isolate individual contribution of daytime variation of AOD and AE to ADRE. Since daytime variation of AE is shown to exert a negligible effect on ADRE calculations, we will only discuss the results from S1, S2 and S3 hereafter.

## 3. Results

### 3.1. Diurnal and seasonal variations of AOD and AE

Hourly percentage departures of AOD and AE between 5:30 and 18:30 at local solar time (LST) in NWC and NCP are presented in Figs. 2–5, respectively. Every data point in these figures represents the mean value of hourly departure relative to the daytime mean. Daytime variations of AOD and AE varied significantly in two regions but showed somewhat similar pattern within stations in each region.

In NWC where dust aerosol is a dominant contributor to AOD, AODs in early morning and later afternoon are nearly always smaller than the daytime mean, on the contrary, AODs during midday (within ~10:00–15:00 LST) are nearly always larger than the daytime means by a few percent to near 20%. This pattern was observed in four seasons although this daytime pattern shows somewhat seasonal and site dependence. A reversed daytime variation of AE to AOD was observed in NWC, i.e., larger AE in early morning and late afternoon but smaller AE during midday. The pattern of daytime variation of AOD and AE here resembles our previous results obtained at Dunhuang (Wang et al., 2004) but a subtle spatial variation of daytime variation is clearly shown in this study. Daytime variability is generally < 20% but occasionally > 40% in some cases, for example, spring AOD in Wulate and autumn AOD in Gaolanshan.

Previous studies showed that diurnal variation of dust storm occurrence frequency in the Mongolian Gobi Desert and semi-arid areas showed an interesting unimodal distribution. About 45% of dust storms occurred in the afternoon, more than double that in the morning and peak outbreaks occurred on 15:00–18:00 LST (Natsagdorj et al., 2008). Since AOD variations in NWC are usually associated with dust storms, daytime variation of AOD in NWC presented here was likely a reflection of diurnal variation of dust storms. For example, daily mean Tazhong and Hotan in spring and summer are much larger than it in other sites because of dust storms (right column in Fig. 2). More frequent dust storms in the afternoon are reflected not only by larger AOD but also larger dust particles (smaller AE). Strong thermal instability due to more solar radiation reaching the surface in the afternoon is likely favorable for the outbreaks of dust storms that obviously needs further study.

A quite different story happens in NCP with regard to the daytime variation of AOD and AE. AOD increases steadily from morning to afternoon. This increase is most outstanding in winter when this AOD increase approaches 40%, i.e., from −20% on 8:00 LST to +20% on 16:00 LST. This pattern is observed not only in urban sites influenced by strong local urban/industrial sources (Beijing and Tianjin) but also in background sites far away from major local urban/industrial sources (Xinglong and Shangdianzi). This fact suggests that the pattern is probably a common feature in NCP that is not likely attributable to changes in emission sources. AE remains stable from morning to afternoon in NCP and most daytime variations are smaller than 5%. Daytime AOD variation in NCP is similar as those observed in urban stations of other continents, for example, in Ispra, Rome, Bucarest in Europe and GSFC, New York City, Buenos-Aires in America (Smirnov et al., 2002).

### 3.2. Effects of daytime variations of AOD and AE on ADRE

Table 2 presents the ADRE differences ($\Delta ADRE_{S2\text{-}S1}$). The results are presented at both the surface and TOA. One thing we should remember here is that ADRE is always negative. If the value in Table 2 is positive (overestimation), it means that the radiation in simulation 1 is smaller than it in simulation 2. In other words, aerosols play a more important role in radiation extinction in simulation 1 than simulation 2. Same for Table 3. ADRE values in simulation 1, 2 and 3 are showed in Tables 4–6, respectively, which will give an intuitive perception. Therefore, positive numbers at first sight in Tables 2 and 3 means more radiation extinction in simulation 1, and vice verse. In NWC, regional mean annual ADRE at the surface is overestimated by 0.31 $Wm^{-2}$ if daytime mean

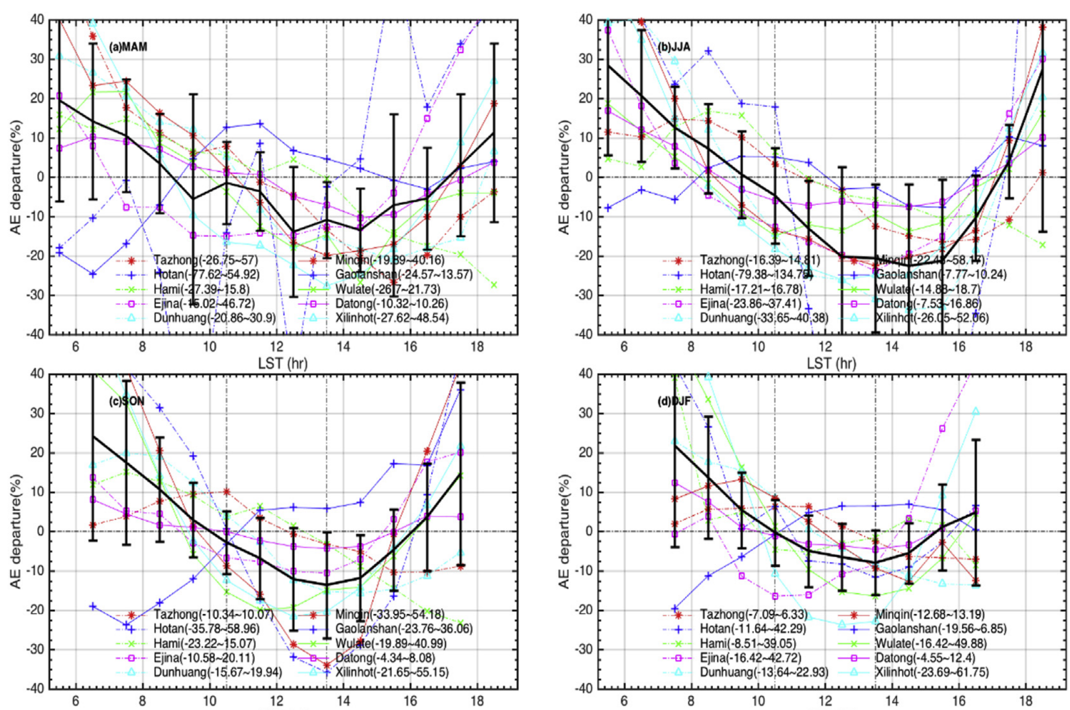


**Fig. 4.** Angstrom Exponent at 10 stations in Northwest China. The minimum and maximum of AE are listed next to site names.

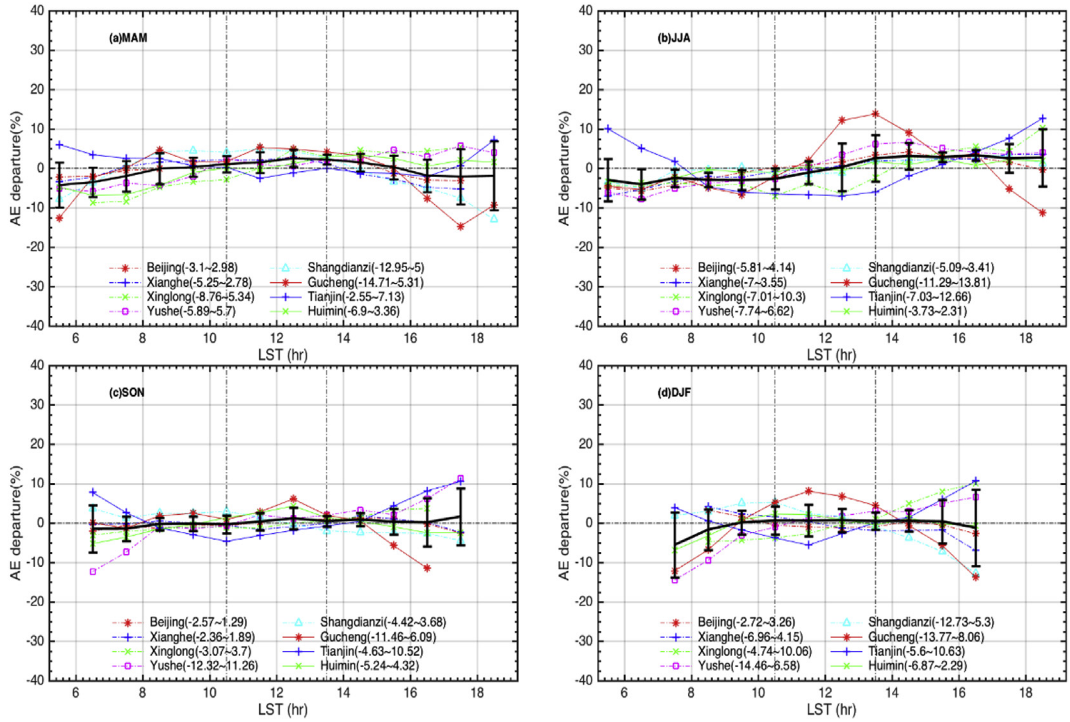


**Fig. 5.** Similar to Fig. 4 but for 8 stations in North China Plain.

**Table 2**
ADRE differences between simulation 2 and simulation 1 at the surface and the TOA.

| | ADRE Difference at the surface ($Wm^{-2}$) | | | | | ADRE Difference at the TOA ($Wm^{-2}$) | | | | |
|---|---|---|---|---|---|---|---|---|---|---|
| | Spring | Summer | Autumn | Winter | Annual | Spring | Summer | Autumn | Winter | Annual |
| NWC | 0.37 | 0.31 | 0.42 | 0.14 | 0.31 | 0.08 | −0.04 | 0.1 | 0.05 | 0.05 |
| Tazhong | 0.72 | 0.6 | 0.3 | 0.06 | 0.42 | 0.18 | 0.03 | 0.08 | 0.02 | 0.08 |
| Hotan | −0.23 | 0.13 | 0.34 | 0.02 | 0.07 | 0.01 | 0.05 | 0.07 | 0.01 | 0.03 |
| Hami | −0.11 | 0 | −0.12 | −0.2 | −0.11 | 0 | 0 | −0.03 | −0.08 | −0.03 |
| Ejina | 0.72 | 0.27 | 0.31 | 0.11 | 0.35 | 0.12 | −0.14 | 0.07 | 0.05 | 0.02 |
| Dunhuang | 0.86 | 0.23 | 0.12 | 0.14 | 0.34 | 0.22 | −0.03 | 0.02 | 0.06 | 0.07 |
| Minqin | 0.44 | 0.56 | 0.63 | −0.2 | 0.36 | 0.16 | −0.07 | 0.15 | −0.07 | 0.04 |
| Gaolanshan | 0.09 | 0.09 | 0.95 | 0.23 | 0.34 | 0.03 | −0.18 | 0.18 | 0.06 | 0.02 |
| Wulate | 0.51 | 0.37 | 0.61 | 0.28 | 0.44 | −0.01 | −0.02 | 0.17 | 0.12 | 0.06 |
| Datong | 0.33 | 0.54 | 0.72 | 0.68 | 0.57 | 0.04 | 0.02 | 0.18 | 0.22 | 0.12 |
| Xilinhot | 0.4 | 0.3 | 0.3 | 0.29 | 0.32 | 0.07 | −0.04 | 0.08 | 0.13 | 0.06 |
| NCP | −0.14 | −0.24 | −0.11 | −0.19 | −0.17 | 0 | 0.01 | −0.03 | −0.08 | −0.03 |
| Beijing | 0.18 | −0.27 | −0.24 | −0.28 | −0.16 | 0.03 | 0.02 | −0.09 | −0.12 | −0.04 |
| Xianghe | 0.13 | −0.82 | −0.26 | −0.28 | −0.31 | 0.07 | −0.12 | −0.09 | −0.12 | −0.07 |
| Xinglong | −0.24 | 0.01 | −0.13 | −0.19 | −0.14 | −0.01 | 0.01 | −0.05 | −0.1 | −0.04 |
| Yushe | −0.58 | −0.97 | −0.56 | −0.28 | −0.6 | −0.06 | 0.02 | −0.17 | −0.11 | −0.08 |
| Shangdianzi | −0.66 | −0.07 | −0.28 | −0.23 | −0.31 | −0.07 | 0.07 | −0.08 | −0.1 | −0.05 |
| Gucheng | −0.04 | −0.06 | 0.04 | −0.42 | −0.12 | 0.01 | −0.02 | 0.02 | −0.17 | −0.04 |
| Tianjin | 0.22 | 0.35 | 0.44 | 0.19 | 0.3 | 0.04 | 0.05 | 0.15 | 0.07 | 0.08 |
| Huimin | −0.17 | −0.05 | 0.11 | −0.04 | −0.04 | 0 | 0.04 | 0.06 | −0.02 | 0.02 |

AOD and AE rather than hourly-resolved values are used in the calculation. $\Delta ADRE_{S2\text{-}S1}$ show somewhat seasonal dependence, varying from 0.14 $Wm^{-2}$ in winter to 0.42 $Wm^{-2}$ in autumn. Regional mean annual ADRE at the TOA is overestimated by 0.05 $W\,m^{-2}$ and the seasonal overestimations vary from $-0.04\,W\,m^{-2}$ in summer to 0.10 $W\,m^{-2}$ in autumn. Although the maximum AOD generally occurs in midday when sun is overhead in NWC, there is still a subtle difference among stations, which leads to slightly different $\Delta ADRE_{S1\text{-}S2}$. For example, a dramatic variation occurs in Wulate where the relative departure of midday AOD approaches 20%, which results in an overestimation of ADRE at the surface and the TOA by 0.44 $Wm^{-2}$ and 0.06 $Wm^{-2}$, respectively, if daytime variation of AOD is replaced by daytime mean AOD. On the contrary, ADRE at the surface is slightly underestimated at Hami. This is because the midday AODs are very close to the daytime average AOD, which is not able to offset the effects of AOD departures in the morning and afternoon on the ADRE calculations. Although substantial daytime variations of AE are observed in NWC, their effects on ADRE estimation is always less than 0.01 $Wm^{-2}$ (not shown). The annual mean ADREs at the surface and TOA in NWC by using AOD and AE at the MODIS overpass time as the diurnal mean are generally smaller than that by using hourly-resolved AOD and AE values ($\Delta ADRE_{S3\text{-}S1} < 0$). It's mainly because AOD at the MODIS overpass time is larger than the daytime

**Table 3**
ADRE differences between simulation 3 and simulation 1 at the surface and the TOA.

| | ADRE Difference at the surface ($Wm^{-2}$) | | | | | ADRE Difference at the TOA ($Wm^{-2}$) | | | | |
|---|---|---|---|---|---|---|---|---|---|---|
| | Spring | Summer | Autumn | Winter | Annual | Spring | Summer | Autumn | Winter | Annual |
| NWC | −0.33 | −1.13 | −0.42 | −0.02 | −0.47 | −0.2 | −0.56 | −0.24 | −0.01 | −0.25 |
| Tazhong | −0.29 | −1.4 | −0.46 | 0.04 | −0.53 | −0.17 | −0.62 | −0.22 | 0.01 | −0.25 |
| Hotan | 1.26 | 0.01 | −0.16 | 0 | 0.28 | 0.52 | 0.01 | −0.11 | 0 | 0.1 |
| Hami | 0.47 | 0.01 | 0.24 | 0.57 | 0.32 | 0.24 | 0 | 0.14 | 0.32 | 0.17 |
| Ejina | −0.92 | −1.65 | −0.54 | 0.07 | −0.76 | −0.55 | −0.87 | −0.32 | 0.02 | −0.43 |
| Dunhuang | −0.92 | −0.54 | −0.06 | 0.26 | −0.31 | −0.47 | −0.33 | −0.06 | 0.12 | −0.18 |
| Minqin | 0.09 | −2.21 | 0.23 | −0.21 | −0.53 | 0.03 | −1.05 | −0.01 | −0.08 | −0.28 |
| Gaolanshan | −0.23 | −1.68 | −1.84 | −1.02 | −1.19 | −0.09 | −0.82 | −0.88 | −0.48 | −0.57 |
| Wulate | −1.33 | −1.26 | −0.66 | 0.46 | −0.7 | −0.76 | −0.63 | −0.4 | 0.22 | −0.39 |
| Datong | −0.63 | −1.48 | −0.56 | −0.56 | −0.81 | −0.33 | −0.69 | −0.33 | −0.32 | −0.42 |
| Xilinhot | −0.77 | −1.07 | −0.39 | 0.21 | −0.51 | −0.42 | −0.56 | −0.24 | 0.09 | −0.28 |
| NCP | 0.53 | 0.83 | −0.42 | −1.23 | −0.07 | 0.22 | 0.3 | −0.16 | −0.6 | −0.06 |
| Beijing | 0.2 | 1.33 | −1.17 | −1.84 | −0.37 | 0.04 | 0.45 | −0.49 | −0.9 | −0.22 |
| Xianghe | 0.47 | 1.05 | −0.52 | −1.9 | −0.23 | 0.17 | 0.37 | −0.2 | −0.95 | −0.15 |
| Xinglong | −0.27 | −0.38 | −0.52 | −1.44 | −0.65 | −0.02 | −0.11 | −0.24 | −0.78 | −0.29 |
| Yushe | 1.35 | 2.76 | 0.09 | −0.92 | 0.82 | 0.54 | 1.06 | 0.11 | −0.43 | 0.32 |
| Shangdianzi | 1.67 | 1.07 | 0.06 | −0.51 | 0.57 | 0.69 | 0.4 | 0.08 | −0.25 | 0.23 |
| Gucheng | 0.23 | −0.32 | −0.75 | −1.29 | −0.53 | 0.09 | −0.09 | −0.32 | −0.56 | −0.22 |
| Tianjin | −0.11 | −0.09 | −0.38 | −1.04 | −0.41 | −0.05 | −0.07 | −0.19 | −0.52 | −0.21 |
| Huimin | 0.74 | 1.26 | −0.15 | −0.84 | 0.25 | 0.28 | 0.4 | −0.05 | −0.39 | 0.06 |

means value that leads to larger ADRE estimations in magnitude there. The bigger deviation AOD, the greater $\Delta ADRE_{S3\text{-}S1}$.

It is suggested that daytime variation of AOD will not result in a significant impact on ADRE if AODs in the morning contrast with AODs in the afternoon (Arola et al., 2013). One would expect negligible effects of daytime variation of AOD on ADRE in NCP since AOD increases steadily from morning to afternoon there. However, the result we calculated here is somewhat differ from this conclusion because AOD pattern is not a perfect mirror around local solar noon. ADREs in NCP are underestimated if hourly-resolved AOD is replaced by the daytime mean value. $\Delta ADRE_{S2\text{-}S1}$ values are −0.17 $Wm^{-2}$ at the surface and −0.03 $Wm^{-2}$ at the TOA, respectively. It's mainly because the turning point of AOD from negative to positive departure mostly occurs later than local noon, which indicates that contrast in ADRE calculations in the morning and afternoon cannot be fully offset when instantaneous ADREs are integrated over all solar zenith angles. There are also some slight differences in $\Delta ADRE_{S2\text{-}S1}$ among sites in NCP, which mainly originates from different turning point of hourly AODs from negative to positive departures. For instance, spring AODs in Xinglong is always less than daytime mean until ~14:00 LST, which results in $\Delta ADRE_{S2\text{-}S1}$ of −0.24 $Wm^{-2}$. If ground-based AOD data at the overpass time of Terra and Aqua is taken as the diurnal average, ADREs at the surface and the TOA are larger than calculations based on hourly-resolved AOD ($\Delta ADRE_{S3\text{-}S1}$ > 0). This result is closely related to the daytime variation pattern of AOD in NCP. AOD at the MODIS overpass time is generally less than the daytime average, which leads to an overestimation

**Table 4**
All ADRE values in simulation 1.

| | ADRE at the surface ($Wm^{-2}$) | | | | | ADRE at the TOA ($Wm^{-2}$) | | | | |
|---|---|---|---|---|---|---|---|---|---|---|
| | Spring | Summer | Autumn | Winter | Annual | Spring | Summer | Autumn | Winter | Annual |
| NWC | −32.21 | −27.75 | −18.98 | −16.56 | −23.88 | −13.57 | −10.53 | −8.51 | −8.6 | −10.3 |
| Tazhong | −54.59 | −48.79 | −25.4 | −18.58 | −36.84 | −21.81 | −17.84 | −11.2 | −9.67 | −15.13 |
| Hotan | −48.76 | −50.54 | −30.26 | −23.11 | −38.17 | −19.61 | −18.45 | −12.75 | −10.93 | −15.43 |
| Hami | −20.93 | −13.82 | −12.58 | −13.72 | −15.26 | −9.55 | −5.62 | −6.21 | −7.68 | −7.26 |
| Ejina | −24.91 | −18.01 | −11.29 | −10.62 | −16.21 | −10.93 | −6.99 | −5.43 | −5.96 | −7.33 |
| Dunhuang | −33.42 | −21.19 | −14.53 | −15.41 | −21.14 | −14.21 | −8.41 | −6.81 | −8.25 | −9.42 |
| Minqin | −31.59 | −29.24 | −21.75 | −16.78 | −24.84 | −13.24 | −10.9 | −9.42 | −8.56 | −10.53 |
| Gaolanshan | −32.55 | −24.24 | −23.8 | −21.87 | −25.62 | −13.48 | −9.24 | −10.04 | −10.64 | −10.85 |
| Wulate | −23.72 | −21.98 | −14.21 | −12.04 | −17.99 | −10.33 | −8.62 | −6.7 | −6.64 | −8.07 |
| Datong | −29.9 | −30.37 | −24.24 | −23.2 | −26.93 | −12.76 | −11.59 | −10.75 | −11.71 | −11.71 |
| Xilinhot | −21.74 | −19.34 | −11.76 | −10.28 | −15.78 | −9.81 | −7.68 | −5.81 | −5.91 | −7.3 |
| NCP | −35.7 | −39.71 | −22.9 | −17.8 | −29.03 | −12.79 | −12.83 | −11.26 | −9.91 | −11.7 |
| Beijing | −39.77 | −43.94 | −24.44 | −15.97 | −31.03 | −13.81 | −14.09 | −12.16 | −8.96 | −12.25 |
| Xianghe | −36.48 | −48.06 | −23.52 | −14.4 | −30.62 | −12.83 | −15.21 | −11.71 | −8.14 | −11.97 |
| Xinglong | −24.57 | −26.54 | −10.84 | −8.69 | −17.66 | −8.73 | −8.99 | −5.62 | −5.1 | −7.11 |
| Yushe | −34.79 | −38.83 | −22.62 | −18.75 | −28.75 | −12.68 | −12.76 | −11.13 | −10.38 | −11.74 |
| Shangdianzi | −31.08 | −33.9 | −19.19 | −13.6 | −24.45 | −11.79 | −11.28 | −9.87 | −8.02 | −10.24 |
| Gucheng | −39.95 | −39.19 | −24.97 | −25.12 | −32.31 | −14.28 | −12.62 | −11.98 | −13.66 | −13.14 |
| Tianjin | −41.54 | −46.71 | −29.61 | −22.53 | −35.1 | −14.78 | −14.7 | −14.26 | −12.43 | −14.04 |
| Huimin | −37.42 | −40.51 | −28.03 | −23.33 | −32.32 | −13.39 | −12.99 | −13.35 | −12.6 | −13.08 |

**Table 5**
All ADRE values in simulation 2.

| | ADRE at the surface ($Wm^{-2}$) | | | | | ADRE at the TOA ($Wm^{-2}$) | | | | |
|---|---|---|---|---|---|---|---|---|---|---|
| | Spring | Summer | Autumn | Winter | Annual | Spring | Summer | Autumn | Winter | Annual |
| NWC | −31.84 | −27.44 | −18.57 | −16.42 | −23.57 | −13.49 | −10.57 | −8.42 | −8.54 | −10.26 |
| Tazhong | −53.86 | −48.19 | −25.1 | −18.52 | −36.42 | −21.62 | −17.81 | −11.12 | −9.65 | −15.05 |
| Hotan | −48.99 | −50.41 | −29.92 | −23.08 | −38.1 | −19.61 | −18.4 | −12.68 | −10.92 | −15.4 |
| Hami | −21.04 | −13.81 | −12.7 | −13.92 | −15.37 | −9.55 | −5.62 | −6.24 | −7.76 | −7.29 |
| Ejina | −24.19 | −17.74 | −10.98 | −10.51 | −15.85 | −10.82 | −7.12 | −5.36 | −5.91 | −7.3 |
| Dunhuang | −32.56 | −20.96 | −14.41 | −15.27 | −20.8 | −14 | −8.45 | −6.79 | −8.19 | −9.36 |
| Minqin | −31.15 | −28.68 | −21.13 | −16.97 | −24.48 | −13.08 | −10.97 | −9.27 | −8.63 | −10.49 |
| Gaolanshan | −32.46 | −24.14 | −22.85 | −21.64 | −25.27 | −13.46 | −9.42 | −9.86 | −10.58 | −10.83 |
| Wulate | −23.2 | −21.61 | −13.6 | −11.77 | −17.54 | −10.34 | −8.64 | −6.54 | −6.52 | −8.01 |
| Datong | −29.57 | −29.83 | −23.52 | −22.52 | −26.36 | −12.72 | −11.57 | −10.58 | −11.49 | −11.59 |
| Xilinhot | −21.34 | −19.04 | −11.46 | −9.99 | −15.46 | −9.74 | −7.72 | −5.73 | −5.78 | −7.24 |
| NCP | −35.84 | −39.95 | −23.01 | −17.99 | −29.2 | −12.78 | −12.82 | −11.29 | −9.99 | −11.72 |
| Beijing | −39.59 | −44.22 | −24.69 | −16.25 | −31.19 | −13.78 | −14.07 | −12.25 | −9.08 | −12.29 |
| Xianghe | −36.35 | −48.89 | −23.78 | −14.68 | −30.92 | −12.76 | −15.33 | −11.8 | −8.26 | −12.04 |
| Xinglong | −24.81 | −26.54 | −10.97 | −8.89 | −17.8 | −8.74 | −8.99 | −5.66 | −5.19 | −7.15 |
| Yushe | −35.37 | −39.81 | −23.18 | −19.03 | −29.34 | −12.74 | −12.74 | −11.3 | −10.49 | −11.82 |
| Shangdianzi | −31.74 | −33.97 | −19.48 | −13.84 | −24.76 | −11.86 | −11.21 | −9.95 | −8.12 | −10.29 |
| Gucheng | −39.98 | −39.25 | −24.93 | −25.54 | −32.42 | −14.26 | −12.64 | −11.97 | −13.83 | −13.17 |
| Tianjin | −41.32 | −46.36 | −29.16 | −22.34 | −34.8 | −14.73 | −14.65 | −14.11 | −12.36 | −13.96 |
| Huimin | −37.59 | −40.56 | −27.92 | −23.37 | −32.36 | −13.39 | −12.95 | −13.3 | −12.62 | −13.06 |

of ADREs. Similar as that in NWC, daytime variation of AE plays a minor role in the estimation of ADRE.

## 4. Conclusions and discussion

A few previous studies have shown that the daytime variability of AOD is significant depending on location and dominant aerosol type. Sites location and aerosol type in NWC and NCP are significantly different. We revealed some interesting daytime variation that have rarely been shown. One of most important impressive results was that substantially different daytime AOD and AE variations have been revealed in NWC and NCP, although some subtle spatial variation in these two regions have also been presented. The former region is dominantly impacted by dust activities, on the contrary, the latter is closely associated with heavy anthropogenic emissions, although dust impacts occasionally occur in spring. These results raised some interesting scientific questions that needs further addressed in future, for example, why daytime variation of AOD show dramatically different stories in these two regions, whether these daytime AOD patterns are close to aerosol source and type, etc. Therefore, this study may have broader impacts.

Aerosol products from the payload of polar satellites, for example, the Moderate Resolution Imaging Spectroradiometer (MODIS) onboard Terra and Aqua, are widely used in the researches of aerosol's effects on climate, although it cannot provide diurnal AOD cycle. Here, we showed that instantaneous AOD at the overpass time differs substantially from daily mean AOD in North China, which may exert

**Table 6**
All ADRE values in simulation 3.

| | ADRE at the surface ($Wm^{-2}$) | | | | | ADRE at the TOA ($Wm^{-2}$) | | | | |
|---|---|---|---|---|---|---|---|---|---|---|
| | Spring | Summer | Autumn | Winter | Annual | Spring | Summer | Autumn | Winter | Annual |
| NWC | −32.54 | −28.88 | −19.4 | −16.58 | −24.35 | −13.77 | −11.09 | −8.76 | −8.61 | −10.56 |
| Tazhong | −54.88 | −50.19 | −25.86 | −18.54 | −37.37 | −21.97 | −18.46 | −11.42 | −9.66 | −15.38 |
| Hotan | −47.5 | −50.53 | −30.42 | −23.11 | −37.89 | −19.09 | −18.44 | −12.87 | −10.93 | −15.33 |
| Hami | −20.46 | −13.81 | −12.34 | −13.15 | −14.94 | −9.31 | −5.62 | −6.07 | −7.37 | −7.09 |
| Ejina | −25.82 | −19.66 | −11.82 | −10.55 | −16.97 | −11.49 | −7.86 | −5.75 | −5.93 | −7.76 |
| Dunhuang | −34.34 | −21.73 | −14.59 | −15.14 | −21.45 | −14.68 | −8.74 | −6.87 | −8.13 | −9.61 |
| Minqin | −31.5 | −31.46 | −21.52 | −16.99 | −25.37 | −13.21 | −11.95 | −9.43 | −8.64 | −10.81 |
| Gaolanshan | −32.78 | −25.91 | −25.64 | −22.89 | −26.81 | −13.58 | −10.06 | −10.92 | −11.12 | −11.42 |
| Wulate | −25.04 | −23.24 | −14.87 | −11.58 | −18.68 | −11.09 | −9.25 | −7.1 | −6.42 | −8.47 |
| Datong | −30.52 | −31.85 | −24.8 | −23.77 | −27.74 | −13.09 | −12.28 | −11.08 | −12.03 | −12.12 |
| Xilinhot | −22.5 | −20.41 | −12.15 | −10.08 | −16.28 | −10.23 | −8.24 | −6.05 | −5.83 | −7.59 |
| NCP | −35.17 | −38.88 | −23.32 | −19.02 | −29.1 | −12.57 | −12.53 | −11.42 | −10.51 | −11.76 |
| Beijing | −39.58 | −42.62 | −25.62 | −17.81 | −31.41 | −13.77 | −13.64 | −12.65 | −9.85 | −12.48 |
| Xianghe | −36.01 | −47.01 | −24.04 | −16.31 | −30.84 | −12.66 | −14.84 | −11.91 | −9.08 | −12.12 |
| Xinglong | −24.83 | −26.92 | −11.36 | −10.14 | −18.31 | −8.75 | −9.1 | −5.85 | −5.87 | −7.4 |
| Yushe | −33.44 | −36.07 | −22.53 | −19.67 | −27.93 | −12.14 | −11.7 | −11.02 | −10.81 | −11.42 |
| Shangdianzi | −29.41 | −32.82 | −19.13 | −14.12 | −23.87 | −11.1 | −10.88 | −9.79 | −8.27 | −10.01 |
| Gucheng | −39.72 | −39.51 | −25.72 | −26.41 | −32.84 | −14.18 | −12.71 | −12.3 | −14.22 | −13.36 |
| Tianjin | −41.65 | −46.8 | −29.99 | −23.57 | −35.5 | −14.83 | −14.77 | −14.45 | −12.95 | −14.25 |
| Huimin | −36.68 | −39.25 | −28.18 | −24.17 | −32.07 | −13.11 | −12.59 | −13.4 | −12.99 | −13.02 |

profound impacts on the evaluation of aerosol's effect on climate, more importantly, caution should be paid to the assessment of aerosol's effect on solar energy application.

Ground-based remote sensing of aerosol optical properties using Sun-photometer is approved to be an important method to accurately characterize aerosol optical properties owing to its wide angular and spectral measurements of solar and sky radiation. AOD and AE data at 18 stations in northern China are used here to reveal daytime variation of AOD and AE pattern. The potential effects of daytime variation of AOD and AE are studied in detail. Major conclusions are as follows.

Distinct daytime variations of AOD and AE are revealed in Northwest China where dust is the dominant aerosol type. AOD pattern in NWC is featured by midday positive departures but negative departures in the morning and afternoon. Daytime AOD relative departure in different sites and seasons varies from −30.26% to 30.28%. The daytime variation of AE in NWC contrasts with that of AOD. AOD increases steadily from morning to afternoon while AE remains stable.

The regional and annual mean ADRE difference between calculations from daytime mean and hourly-resolved AOD and AE is 0.31 $Wm^{-2}$ at the surface while it is 0.05 $Wm^{-2}$ at the TOA in NWC. ADRE in NWC will be underestimated at both the surface and TOA if instantaneous AOD and AE during the MODIS overpass time is taken as the daytime mean.

In NCP, the annual mean ADRE differences at the surface and TOA are −0.17 $Wm^{-2}$ and -0.03 $Wm^{-2}$ if daytime mean AOD and AE are used to replace hourly-resolved values. Instantaneous AODs at the MODIS overpass time are less than the daytime means which results in an underestimation of ADRE (−0.07 $Wm^{-2}$ at the surface and −0.06 $Wm^{-2}$ at the TOA).

Daytime variation of AE plays a minor role in the calculation of ADRE. In most cases, difference in ADREs calculated from daytime mean and hourly-resolved AE does not exceed 0.01 $Wm^{-2}$.

## Acknowledgements

This work is supported by the National key research and development program of China (2016YFC0200403 and 2017YFA0603504), the National Science Foundation of China (41475138, 41675033, 41475026, 91644217, 41590874) and CAMS Basis Research Project (2017Z11, 2016Z001 & 2014R17), the Climate Change Special Fund of CMA (CCSF201504).

## References

Arola, A., Eck, T.F., Huttunen, J., et al., 2013. Influence of observed diurnal cycles of aerosol optical depth on aerosol direct radiative effect. Atmos. Chem. Phys. 13 (15), 7895–7901. https://doi.org/10.5194/acp-13-7895-2013.

Che, H., Zhang, X., Chen, H., et al., 2009. Instrument calibration and aerosol optical depth validation of the China Aerosol Remote Sensing Network. J. Geophys. Res.: Atmosphere 114 (D3). https://doi.org/10.1029/2008JD011030.

Che, H., Wang, Y., Sun, J., 2011. Aerosol optical properties at Mt. Waliguan observatory, China. Atmos. Environ. 45 (33), 6004–6009. https://doi.org/10.1016/j.atmosenv.2011. 07. 050.

Che, H., Wang, Y., Sun, J., et al., 2013. Variation of aerosol optical properties over the Taklimakan Desert in China. Aerosol Air Qual. Res. 13, 777–785. https://doi.org/10.4209/aaqr.2012.07.0200.

Che, H., Xia, X., Zhu, J., et al., 2014. Column aerosol optical properties and aerosol radiative forcing during a serious haze-fog month over North China Plain in 2013 based on ground-based sunphotometer measurements. Atmos. Chem. Phys. 14 (4), 2125–2138. https://doi.org/10.5194/acp-14-2125-2014.

Che, H., Xia, X., Zhu, J., et al., 2015a. Aerosol optical properties under the condition of heavy haze over an urban site of Beijing, China. Environ. Sci. Pollut. Control Ser. 22 (2), 1043–1053. https://doi.org/10.1007/s11356-014-3415-5.

Che, H., Zhang, X.Y., Xia, X., et al., 2015b. Ground-based aerosol climatology of China: aerosol optical depths from the China Aerosol Remote Sensing Network (CARSNET) 2002–2013. Atmos. Chem. Phys. 15 (13), 7619–7652. https://doi.org/10.5194/acp-15-7619-2015.

Christopher, S.A., Wang, J., Ji, Q., et al., 2003. Estimation of diurnal shortwave dust aerosol radiative forcing during PRIDE. J. Geophys. Res.: Atmos. 108 (D19). https://doi.org/10.1029/2002JD002787.

Holben, B.N., Eck, T.F., Slutsker, I., et al., 1998. AERONET—a federated instrument network and data archive for aerosol characterization. Rem. Sens. Environ. 66 (1), 1–16. https://doi.org/10.1016/S0034-4257(98)00031-5.

Holben, B.N., Tanre, D., Smirnov, A., et al., 2001. An emerging ground-based aerosol climatology: aerosol optical depth from AERONET. J. Geophys. Res.: Atmos. 106 (D11), 12067–12097. https://doi.org/10.1029/2001JD900014.

Kuang, Y., Zhao, C., Tao, J., et al., 2015. Diurnal variations of aerosol optical properties in the North China Plain and their influences on the estimates of direct aerosol radiative effect. Atmos. Chem. Phys. 15 (10), 5761–5772. https://doi.org/10.5194/acp-15-5761-2015.

Kaufman, Y.J., Holben, B.N., Tanré, D., et al., 2000. Will aerosol measurements from Terra and Aqua polar orbiting satellites represent the daily aerosol abundance and properties? Geophys. Res. Lett. 27 (23), 3861–3864. https://doi.org/10.1029/2000GL011968.

Natsagdorj, L., Jugder, D., Chung, Y., 2003. Analysis of dust storms observed in Mongolia during 1937-1999. Atmos. Environ. 37, 1401–1411.

Peterson, J.T., Flowers, E.C., Berri, G.J., et al., 1981. Atmospheric turbidity over central North Carolina. J. Appl. Meteorol. 20 (3), 229–241 https://doi.org/10.1175/1520-0450(1981)020229:ATOCNC > 2.0.CO;2.

Ricchiazzi, P., Yang, S., Gautier, C., et al., 1998. SBDART: a research and teaching software tool for plane-parallel radiative transfer in the Earth's atmosphere. Bull. Am. Meteorol. Soc. 79 (10), 2101–2114 1520-0477(1998)079 < 2101:SARATS > 2.0.CO;2.

Smirnov, A., Holben, B.N., Eck, T.F., et al., 2002. Diurnal variability of aerosol optical depth observed at AERONET (Aerosol Robotic Network) sites. Geophys. Res. Lett. 29 (23). https://doi.org/10.1029/2002GL016305.

Wang, J., Christopher, S.A., Reid, J.S., et al., 2003. GOES 8 retrieval of dust aerosol optical thickness over the Atlantic Ocean during PRIDE. J. Geophys. Res.: Atmos. 108 (D19). https://doi.org/10.1029/2002JD002494.

Wang, J., Xia, X., Wang, P., et al., 2004. Diurnal variability of dust aerosol optical thickness and Angström exponent over dust source regions in China. Geophys. Res. Lett. 31 (8). https://doi.org/10.1029/2004GL019580.

Wang, J., Christopher, S.A., Nair, U.S., et al., 2006. Mesoscale modeling of Central American smoke transport to the United States: 1."Top-down" assessment of emission strength and diurnal variation impacts. J. Geophys. Res.: Atmosphere 111 (D5). https://doi.org/10.1029/2005JD006416.

Wang, J., Martin, S.T., 2007. Satellite characterization of urban aerosols: importance of including hygroscopicity and mixing state in the retrieval algorithms. J. Geophys. Res.: Atmos. 112 (D17). https://doi.org/10.1029/2006JD008078.

Wang, Z., Liu, D., Wang, Y., et al., 2015. Diurnal aerosol variations do affect daily averaged radiative forcing under heavy aerosol loading observed in Hefei, China. Atmos. Meas. Tech. 8 (7), 2901–2907. https://doi.org/10.5194/amt-8-2901-2015.

Xia, X., Chen, H., Wang, P., et al., 2006. Variation of column-integrated aerosol properties in a Chinese urban region. J. Geophys. Res.: Atmos. 111 (D5). https://doi.org/10.1029/2005JD006203.

Xia, X., Che, H., Zhu, J., et al., 2016. Ground-based remote sensing of aerosol climatology in China: aerosol optical properties, direct radiative effect and its parameterization. Atmos. Environ. 124, 243–251. https://doi.org/10.1016/j.atmosenv.2015.05.071.

Xu, H., Guo, J., Ceamanos, X., et al., 2016. On the influence of the diurnal variations of aerosol content to estimate direct aerosol radiative forcing using MODIS data. Atmos. Environ. 141, 186–196. https://doi.org/10.1016/j.atmosenv.2016.06.067.

Zhang, Y., Yu, H., Eck, T.F., et al., 2012. Aerosol daytime variations over North and South America derived from multiyear AERONET measurements. J. Geophys. Res.: Atmos. 117 (D5). https://doi.org/10.1029/2011JD017242.

Zhu, J., Che, H., Xia, X., et al., 2014. Column-integrated aerosol optical and physical properties at a regional background atmosphere in North China Plain. Atmos. Environ. 84, 54–64. https://doi.org/10.1016/j.atmosenv.2013.11.019.